Microsyst Technol
DOI 10.1007/s00542-015-2647-8

TECHNICAL PAPER

Structural, optical and electrical properties of $Cu_2Zn_{1-x}Cd_xSnS_4$ quinternary alloys nanostructures deposited on porous silicon

A. S. Ibraheam[1] · Y. Al-Douri[1,2] · J. M. S. Al-Fhdawi[3] · Hamid S. AL-Jumaili[4] · K. D. Verma[5] · U. Hashim[1] · R. M. Ayub[1] · A. Rahim Ruslinda[1] · M. K. Md Arshad[1] · A. H. Reshak[6,7] · S. B. Abd Hamid[8]

Received: 3 June 2015 / Accepted: 28 July 2015

Abstract The $Cu_2Zn_{1-x}Cd_xSnS_4$ quinternary alloy nanostructures with different Cd contents were grown using spin coating technique on porous silicon (63.93 %) substrate. The structural properties of $Cu_2Zn_{1-x}Cd_xSnS_4$/PS were investigated by X-ray diffraction and field emission-scanning electron microscope (FE-SEM). The optical properties studied through photoluminescence technique, indicated that the band gap is shifted as Cd content increases from 1.84 eV at x = 0 to 1.76 eV at x = 1. The electrical characterization of the Ag/n-PS/$Cu_2Zn_{1-x}Cd_xSnS_4$/Ag diode through current to voltage (I–V) characterization shows the highest photo-response of (value if any) at $Cu_2Zn_{0.4}Cd_{0.6}SnS_4$ composition.

✉ Y. Al-Douri
yaldouri@yahoo.com

1 Institute of Nano Electronic Engineering, University Malaysia Perlis, 01000 Kangar, Perlis, Malaysia

2 Physics Department, Faculty of Science, University of Sidi-Bel-Abbes, 22000 Sidi Bel Abbès, Algeria

3 Department of Physics, College of Science, University of Anbar, Ramadi, Iraq

4 Department of Physics, College of Education for Pure Science, University of Anbar, Ramadi, Iraq

5 Material Science Research Laboratory, Department of Physics, S. V. College, Aligarh, UP 202001, India

6 New Technologies, Research Centre, University of West Bohemia, Univerzitni 8, 306 14 Pilsen, Czech Republic

7 Center of Excellence Geopolymer and Green Technology, School of Material Engineering, University Malaysia Perlis, 01007 Kangar, Perlis, Malaysia

8 Nanotechnology and Catalysis Research Center (NANOCAT), University of Malaya, 50603 Kuala Lumpur, Malaysia

1 Introduction

A kesterite structure type of Cu_2ZnSnS_4 (CZTS) is a potential absorber material as thin film solar cells due to presence of naturally abundant, inexpensive, efficient and environment friendly elements. It is known that CZTS has a direct band gap between 1.45 and 1.6 eV with high absorption coefficient over 10^4 cm^{-1} (in visible light), intrinsic p-type conductivity and low thermal conductivity (Katagiri et al. 2001; Kamoun et al. 2007; Levcenco et al. 2012). These properties promote CZTS as a good candidate for photovoltaic materials. The predicted theoretical efficiency of CZTS based solar cell is larger than 30 % (Daranfed et al. 2012; Todorov et al. 2010; Guo et al. 2009; Katagiri et al. 2009). Efficiency up to 6.77 % has been already reached in solar cells produced with CZTS as absorber layer (Canham 1997). Silicon substrates have high quality single crystal with nearly defect free, very low volume density of impurities and controlled amount of dopants. It may be prepared flat on the atomic scale by standard methods that lead to porous silicon (PS) formation (Yerokhov and Melnyk 1999). The PS is attractive for solar cell applications due to its efficient antireflection coatings and other properties such as band gap broadening (Schirone et al. 1997), wide absorption spectrum (Menna et al. 1997) and optical transmission range (700–1000 nm) (Schirone et al. 1998). It can also be used for surface passivation and texturization (Cláudia et al. 2008).

Al-Douri et al. (2011) have calculated the energy gap of Si that is found to be indirect using empirical pseudo potential method (EPM). They have investigated features such as refractive index, optical dielectric constant, bulk modulus, elastic constants and short-range force constants, in addition to the shear modulus, Young's modulus, Poisson's ratio

Published online: 06 August 2015

and Lame's constants for both Si and PS. The Debye temperature of PS was estimated from the average sound velocity. Cu_2ZnSnS_4 (CZTS) film was fabricated by sulfurization of two stacked layers of Cu(Zn,Sn) (CZT) alloy precursors by Hong and Kim (2013). The sulfurization was performed in an evacuated and sealed quartz ampoule with sulphur powder, in which samples were annealed at 450, 500, or 550 °C for 1 h. The energy band gap of CZTS absorber was determined to be 1.370–1.414 eV. While, Xinkun et al. (2012) have prepared Sn/Cu/ZnS by evaporation on soda lime glass at room temperature, and then polycrystalline thin films of Cu_2ZnSnS_4 (CZTS) were produced by sulfurizing the precursors in a sulfur atmosphere at a temperature of 550 °C for 3 h. The experimental results show that, when the ratios of [Cu]/([Zn] + [Sn]) and [Zn]/[Sn] in the CZTS are 0.83 and 1.15, the CZTS thin films possess an absorption coefficient larger than 4.0×10^4 cm^{-1} in the energy range 1.5–3.5 eV, and a direct band gap (1.47 eV). Therefore, the CZTS thin films are suitable for absorption layers of solar cells. Accordingly, successful experiments have discovered that electrochemical and chemical dissolution enable the silicon wafers to emit light in red luminescence (Canham 1990). During the last years, the optical properties of PS have become a very intense area of research.

The prime aim of this work is to study the structural properties given by X-ray diffraction (XRD) and field emission-scanning electron microscope (FE-SEM), and optical properties of $Cu_2Zn_{1-x}d_xSnS_4$ quaternary alloy nanostructures by PL, in addition to investigate the electrical properties of Ag/n-PS/$Cu_2Zn_{1-x}Cd_xSnS_4$/Ag diode at x = 0, 0.6, 1 for photodetector applications through (I–V) characterization. The paper is organized as the followings; Sect. 2 details the experimental procedure. The results and discussion are elaborated in Sect. 3. Finally, conclusion is summarised in Sect. 4.

2 Experimental

Spin coating technique is used to deposit the $Cu_2Zn_{1-x}d_x$-SnS_4 quaternary alloy nanostructures onto n-type PS substrate. The n-PS substrate was prepared as reported by Abd et al. (2013) where the optimal case (63.93 %) was selected. First the solution of $Cu_2Zn_{1-x}Cd_xSnS_4$ precursors was prepared by dissolving copper (II) chloride dihydrate (0.3 M), zinc (II) chloride dihydrate (0.3 M), tin (II) chloride dehydrate (0.3 M), cadmium (II) chloride (0.3 M), thiourea (0.6) was dissolved in 2-methoxyethanol and monoethanolamine (MEA—as a stabilizer) was added as a stabilizer. The mole ratios of Cu, (Zn + Cd), Sn, and S in the solution were 2:1:1:4. For obtaining the solution with different Cd content (x), the mole ratios of Cd to (Zn + Cd) in the solution vary according to the value of x as 0, 0.6, and 1. The solution was stirred at 50 °C to completely dissolve the metal compounds during stirring the milk solution became yellow in colour. Afterthat, the solution was dropped onto optimal etching substrate, which was rotating at 2500 rpm for 30 s. After deposition by spin coating, the nanostructures were dried at 250 °C for 80 min on hot plate. The coating and drying processes were repeated for seven times to obtain 1 μm thickness. The thickness measurement has been carried out using the weight method by:

$$t = \frac{\Delta m}{A \times \rho},$$

where t is thickness, Δm is difference of substrate weight (substrate after deposition − substrate before deposition), A is area of sample and ρ is density of deposited material. Finally, heat treatment was conducted in an elevator furnace under N_2 gas flow (5 % gas atmosphere) for 1 h at 300 °C and after annealing, the samples was cooled to below 40 °C in the chamber. Afterthat, Ag metal contacts were formed on $Cu_2Zn_{1-x}Cd_xSnS_4$ quaternary alloy nanostructures with Cd content equals 0, 0.6, 1. PVD-HANDY/2STE (Vaksis Company, USA) vacuum thermal evaporation in the pressure of 4.5×10^5 Torr was used for deposition on oxidized silicon, and the contacts were formed in the form of zigzag with 5 mm length and 100 nm thickness as shown in Fig. 1. The contact area of the diode was found to be 3.14×10^2 cm^2. This work is analysed by XRD analysis as carried out on the as-deposited films to check the crystalline structure using (Philips PW 1710 X-ray diffractometer, USA), which record the intensity as a function of Bragg's angle in 2θ-range from 20–60° using Cu kα (λ = 1.5406 Å). Photoluminescence (PL) spectroscopy system (Perkin Elmer Lambda 950, USA) was using He-Cd laser with the wavelength (λ) of 325 nm. Surface morphologies for $Cu_2Zn_{1-x}Cd_xSnS_4$ quinternary alloy nanostructures were investigated by FE-SEM system (NOVA NANO SEM 450, USA). For the current to voltage (I–V) characterization, the fabricated device was connected in parallel with the Kiethly 2400 source meter, USA. The reading was recorded from −6 to 6 V. For current to time (I–t) analysis, the device was connected in series with the multimeter and

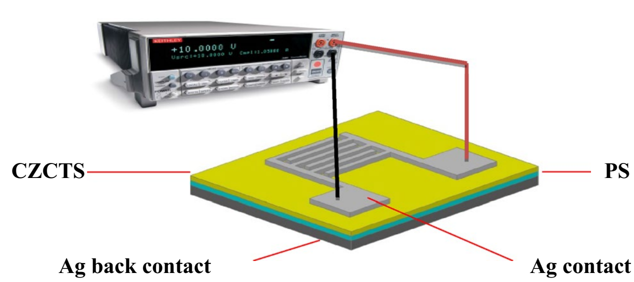

Fig. 1 p–n junction

the value was recorded by switching the LED on and off. The wavelength and power of the LED used for conducting the experiment were 490 nm wavelength and 2 mW power, respectively.

3 Results and discussion

The XRD patterns of $Cu_2Cd_xZn_{1-x}SnS_4$ quinternary alloy nanostructures with x = 0, 0.6 and 1 deposited on PS prepared at the current density of 5 mA/cm^2 for 120 min are shown in Fig. 2 The major diffraction peaks appear at 2θ = 28.757°, 32.313°, 34.275° and 47.30° which can be attributed to the (112), (200), (004) and (220) planes of kesterite phase of Cu_2ZnSnS_4 (ICDD PDF2008, 01-075-4122) and stannite phase of Cu_2CdSnS_4 (ICDD PDF2008, 00-029-0537). It shows the highest (112) diffraction peak at x = 1. The peaks are shifted to the lower angle side with increasing Cd content in the CZCTS solid solutions, which was attributed to the increasing lattice constant. This was because the radius of Cd ion (1.53 Å) is larger than that of Zn (1.33 Å) as supported by previous work (Ibraheam et al. 2015). The simplest possibility is that Cd substitutes other metals at their sites in crystal lattice of $Cu_2Cd_xZn_{1-x}SnS_4$ quinternary alloy nanostructures. As the theoretical calculated substitution energies of Cd atoms at Cu, Sn and Zn atom sites in CZTS lattice are E_{sub} (Cd_{Cu}) = 0.69 eV, E_{sub} (Cd_{Sn}) = 1.07 eV and E_{sub}(Cd_{Zn}) = 0.53 eV (Maeda et al. 2012), the most likely is the isoelectronic substitution of Cd at the Zn site. Lattice constants a and c were calculated from XRD data for the (112) plane, which are given in Table 1;

$$\left(1/d^2\right) = \left(\left(h^2 + k^2\right)/\, a^2\right) + \left(l^2/\, c^2\right), \tag{1}$$

where hkl are the Miller indices, a and c are the lattice constants. The interplane distance (d) was calculated for all of CZCTS nanostructures using Bragg's diffraction equation (Ibraheam et al. 2015)

$$d = n\lambda/2\sin\theta, \tag{2}$$

where λ is wavelength of XRD using (λ = 1.5406 Å) and θ is the Bragg's angle.

The crystallite size (D) was calculated by Scherrer's formula (Ibraheam et al. 2015)

$$D = k\lambda/\beta\cos\theta. \tag{3}$$

where k is a constant, taken to be 0.94, and β is the full width at half maximum (FWHM).

It is known that the bulk modulus is a reflectance of the materials stiffness, which is important in different industries. Many authors (Sherry and Kumar 1991; Tallon 1980; Al-Douri et al. 2002, 2005; Al-Douri 2003, 2012) have made various efforts to explore thermodynamic properties of solids. In these studies, authors have examined the

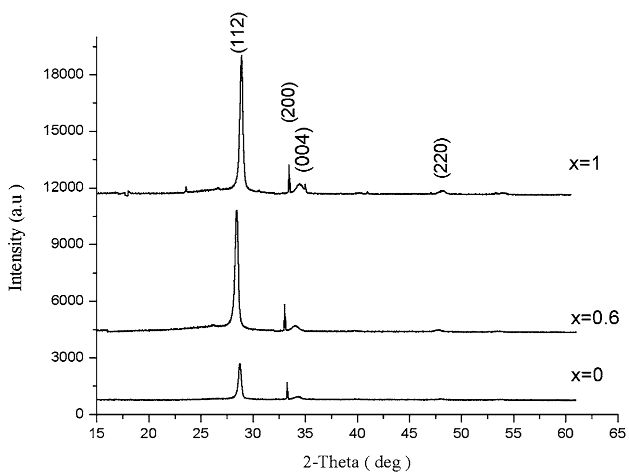

Fig. 2 XRD patterns of $Cu_2Zn_{1-x}Cd_xSnS_4$ quinternary alloy nanostructures at different Cd contents, x = 0, 0.6, 1

Table 1 The structural properties of $Cu_2Zn_{1-x}Cd_xSnS_4$ quinternary alloy nanostructures using XRD for different Cd contents, x = 0, 0.6, 1

X	Peak (θ)	Particle size (nm)	D_{hkl} (112) (Å)	Lattice constants (Å)	Bulk modulus (GPa)
0	28.757	30.71	3.463	a = 5.429 a = 5.427[a] c = 10.856 c = 10.848[a]	84.96
0.6	28.736	41.80	3.558	a = 5.525 c = 10.906	79.90
1	28.723	53.52	3.703	a = 5.586 a = 5.487[b] c = 11.992 c = 11.389[c]	76.89

[a] Ref. (Ibraheam et al. 2015) exp.

[b] Ref. (Guan et al. 2013) exp.

[c] Ref. (Matsushita et al. 2000) exp.

thermodynamic properties such as the inter-atomic separation and the bulk modulus of solids with different approximations and best-fit relations (Al-Douri et al. 2002, 2005; Al-Douri 2003, 2012). It has become possible to compute with great accuracy an important number of structural and electronic properties of solids. The ab initio calculations are complex and require significant effort. Therefore, more empirical approaches have been developed (Phillips 1973; Harison 1989) to compute properties of materials. In many cases, the empirical methods offer the advantage of applicability to a broad class of materials and to illustrate trends. In many applications, these empirical approaches do not give highly accurate results for each specific material, but are still very useful. Cohen (1985) has established an empirical formula for calculation of the bulk modulus B_0; based on the nearest-neighbor distance. His result is in agreement with experimental values. Lam et al. (Lam et al. 1987) have derived an analytical expression for the bulk modulus from the total energy. This expression is different in structure from the empirical formula but gives similar numerical results. Also, they have obtained an analytical expression for the pressure derivative B_0 of the bulk modulus. Our group (Al-Douri et al. 2004) used a concept based on the lattice constant to establish an empirical formula for the calculation of the bulk modulus. The results are in good agreement with experimental data and other calculations. The theory yields a formula with two attractive features. Only the lattice constant is required as input, the computation of B_0 itself is trivial. Consideration of hypothetical structure and simulation of the experimental conditions are required to make practical use of this formula.

The aim is to see how a qualitative concept, such as the bulk modulus, can be related to the lattice constant. It was argued that the dominant effect is the degree of covalency characterized by Phillips' homopolar gap E_h (Phillips 1973), and one reason for presenting these data in this work is that the validity of our calculations that is not restricted in computed space. We thus believe that the data will prove valuable for future work in this field. An important reason for studying B_0 is the observation of clear differences between the lattice constants for CZCST quinternary alloy nanostructures as seen in Table 1. The basis of our model is the lattice constant as seen in Table 1. Fitting of these data gives the following empirical formula (Al-Douri et al. 2004):

$$B_0 = \left[3000 - 100\lambda\right] \left(\frac{a}{2}\right)^{-3.5} \tag{4}$$

where a is the lattice constant (in Å) and λ is an empirical parameter which accounts for the effect of ionicity; λ = 0;

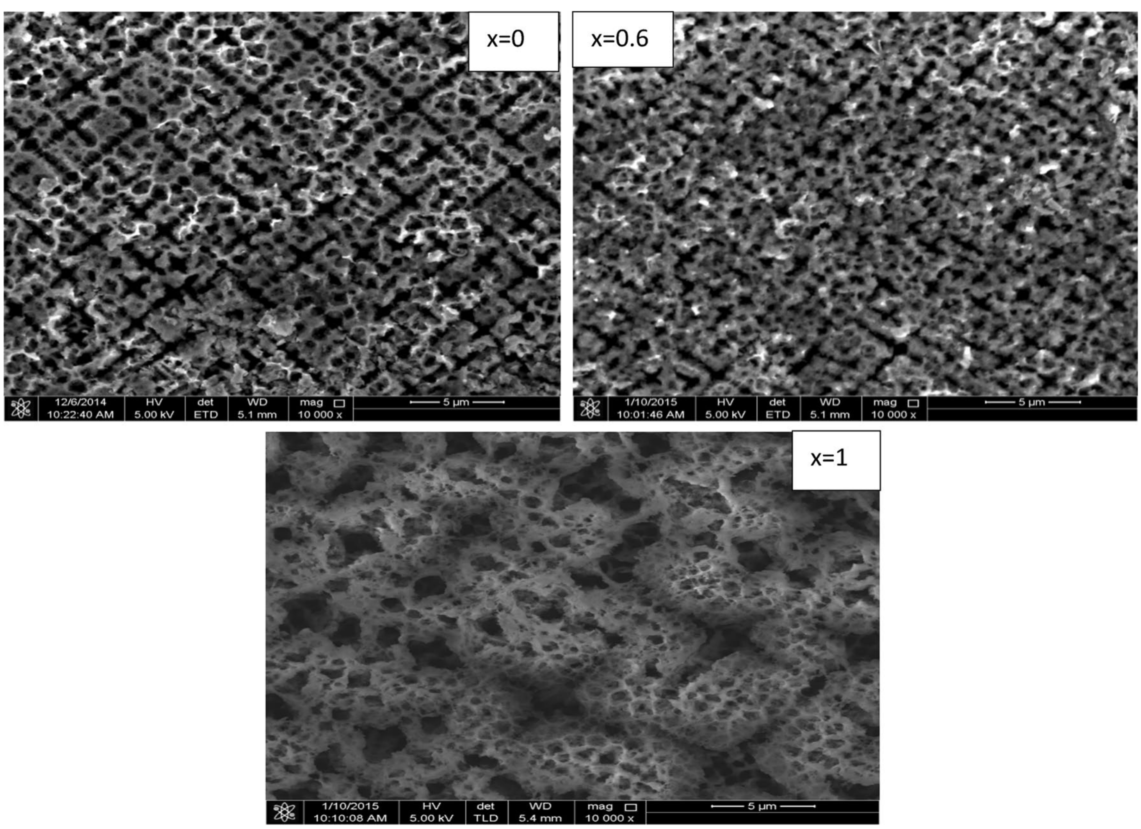

Fig. 3 FE-SEM images of $Cu_2Zn_{1-x}Cd_xSnS_4$ quinternary alloy nanostructure grown on PS at different Cd contents, x = 0, 0.6, 1

1, 2 for group IV, III–V, and II–VI semiconductors, respectively. In Table 1, the calculated bulk modulus values are investigated. We may conclude that the present bulk moduli calculated in a different way than the definition of Cohen exhibit the same chemical trends as those found for their constituents. It is observed that Cd content is proportion inversely with the stiffness of CZCTS quinternary alloy nanostructures.

Figure 3 shows top-view of FE-SEM images of $Cu_2Zn_{1-x}Cd_xSnS_4$ quinternary alloy nanostructures grown on PS (63.93 %) with different Cd content (x). At x = 0, the surface has multiple pores among the grains. The number of pores decreases as the Cd content increases. The sample grown with x = 0.6 clearly to show the largest grain size. This is because of the adjacent $Cu_2Zn_{1-x}Cd_xSnS_4$ grains are tended to merge into larger ones as Cd content increases. Contrary, at x = 1, the grains have extremely small pores. In addition, the top-view image of as prepared n-PS/$Cu_2Zn_{1-x}Cd_xSnS_4$ reveals a uniform distribution of pores.

The PL spectra of $Cu_2Zn_{1-x}Cd_xSnS_4$ quinternary alloy nanostructure deposited on PS prepared at the current density of 5 mA/cm^2 for 120 min are shown in Fig. 4. The peak position (λ_{max}) and the full width at half maximum (FWHM) of the band gap are shifted with increasing Cd content from $\lambda_{max} = 672.87$ nm (x = 0) to 677 nm (x = 0.6) to 701 nm (x = 1) corresponding to energy gaps 1.84 eV (x = 0), 1.83 eV (x = 0.6) and 1.76 eV (x = 1), respectively. The shifting is is due to substituting Zn atoms with Cd atoms to produce a lower energy gap, because ZnS has a direct energy gap (3.62 eV) (Hu et al. 2013; Luque et al. 2013).The current-to-voltage (I–V) characteristics of the fabricated devices in dark and white light (tungsten lamp) under 460 nm for the Ag/n-PS/$Cu_2Zn_{1-x}CdSnS_4$/Ag diode at x = 0, 0.6, 1 are shown in Fig. 5. The photocurrent ratio between I_{dark} and I_{ph} is increased with increasing Cd content. The photosensitivities of the heterojunctions were calculated by the equation

$$S = \frac{I_{ph} - I_{dark}}{I_{dark}} \times 100\ \% \tag{5}$$

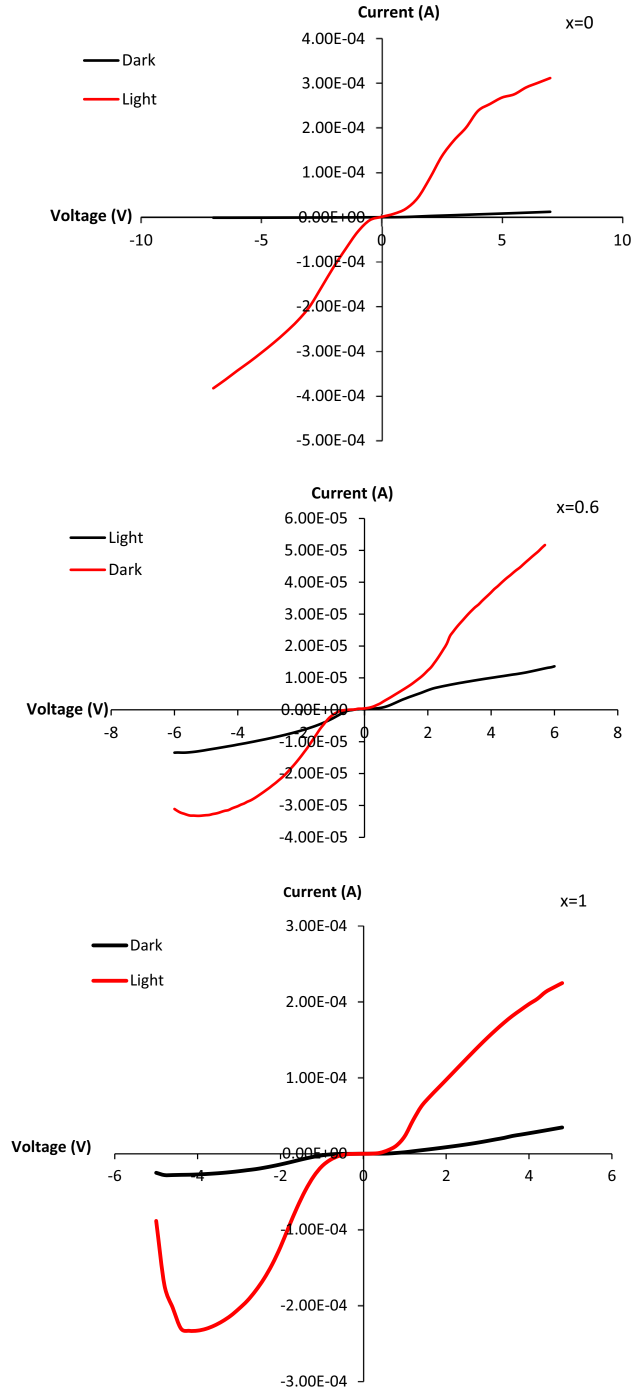

Fig. 5 I–V characteristics of the Ag/n-PS/$Cu_2Zn_{1-x}Cd_xSnS_4$/Ag diode at different Cd contents, x = 0, 0.6, 1. The measurements are in dark and under white light

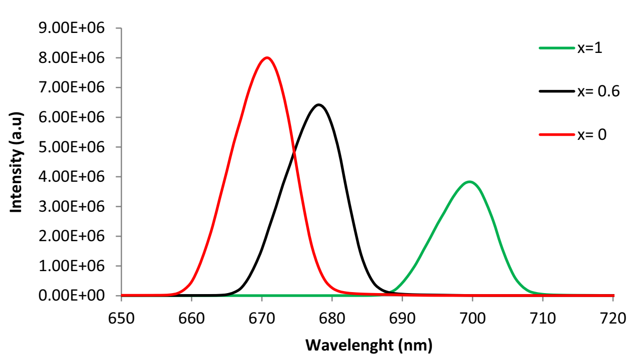

Fig. 4 PL of $Cu_2Zn_{1-x}Cd_xSnS_4$ quinternary alloy nanostructures at different Cd contents, x = 0, 0.6, 1

Table 2 Photoresponse properties of the Ag/n-PS/$Cu_2Zn_{1-x}Cd_xSnS_4$/Ag diode 1 at bias voltage 3 V and wavelength 490 nm

X	I_{dark} (A)	I_{ph} (A)	I_{ph}/I_{dark}	S_{ph} (%)
0	1.08×10^{-5}	4.13×10^{-5}	3.82	282.40
0.6	7.35×10^{-6}	25×10^{-5}	34.01	3401.36
1	3.28×10^{-5}	2.19×10^{-4}	6.67	567.68

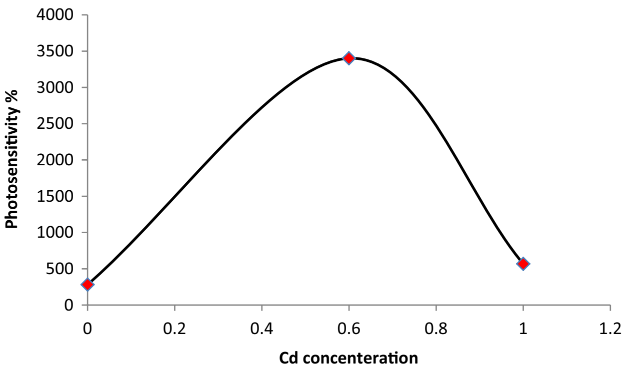

Fig. 6 Photosensitivity o of the Ag/n-PS/$Cu_2Zn_{1-x}Cd_xSnS_4$/Ag diode at different Cd contents, x = 0 0.0.6, 1

Based on the I–V curve (Fig. 5) and Eq. (5), the I_{dark} and I_{ph} are listed in Table 2. The dark current is decreased with increasing Cd content. It can be attributed to the improvement of the crystalline properties with increasing of Cd content, that leading to the reduction of the structural defects of the surface that guide to improvement in the electrical properties. Figure 6 shows that the photosensitivity increases as Cd content increases to 3401.36 for x = 0.6 and decreases to 567.68 to x = 1 (Table 2). The photo-to-dark current ratio was achieved at maximum of 34.01 for x = 0.6 compared with 3.82 for x = 0 (Table 2). No more increase in the output current with increasing Cd content up to x = 1, this is related to the substitution impurities relating to trapping centre production which inversely affect the photocurrent. The photocurrent values of $Cu_2Zn_{0.4}Cd_{0.6}SnS_4$ quinternary alloy nanostructures are higher than their endmembers Cu_2ZnSnS_4 and Cu_2CdSnS_4.

To confirm the better performance of the photodetector and reproducibility of the device (Ag/n-PS/$Cu_2Zn_{1-x}Cd_xSnS_4$/Ag), it was examined by cyclically switching the white light on and off. Figure 7 shows the I_{ph} as a function of time intervals (I–t) of $Cu_2Zn_{1-x}Cd_xSnS_4$ quinternary alloy nanostructures at x = 0, 0.6, 1. I_{ph} sharply increased/decreased to reach the maximum/minimum under 490 nm white light on/off. The $Cu_2Zn_{1-x}Cd_xSnS_4$ quinternary alloys nanostructures at x = 0.6 (Fig. 7b) shows better performance than at x = 0, 1 (Fig. 7a, c). The result indicated

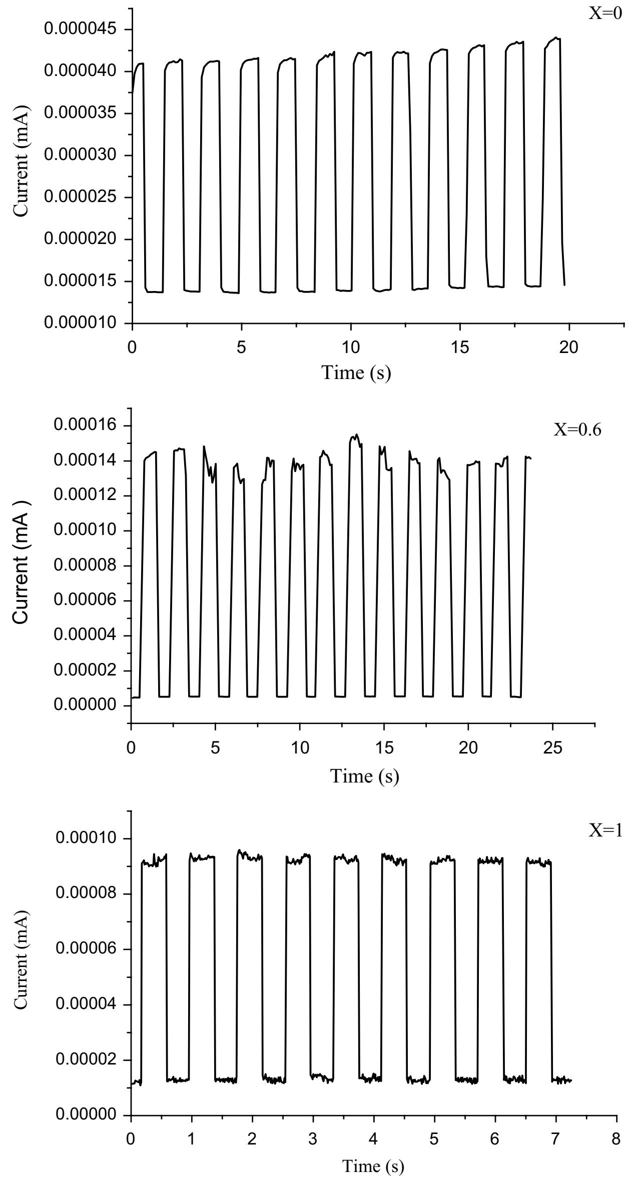

Fig. 7 Photocurrent response spectra of Ag/n-PS/$Cu_2Zn_{1-x}Cd_xSnS_4$/Ag diode different Cd contents, x = 0, 0.6, 1 with white illumination, 490 nm turned on and off repeatedly at bias voltage 3 V

Table 3 Response and decay time correspond to I_{ph}/I_{dark} ratio of Ag/n-PS/$Cu_2Zn_{1-x}Cd_xSnS_4$/Ag diode

X	Response time (t_{Res}) (s)	Decay time (t_{Rec}) (s)	I_{ph}/I_{dark}
0	0.036	0.025	2.85
0.6	0.010	0.011	14
1	0.021	0.017	8.18

an improvment with increasing Cd content, x = 0.6. The I_{ph}/I_{dark} ratio was 2.85, 14 and 8.18 for x = 0, 0.6 and 1, respectively as given in Table 3. The calculated response time (t_{Res}) and decay time (t_{Rec}) using 490 nm and 3 V show that all values are decreased with increasing of Cd content indicating an improved photoresponse. Performance of $Cu_2Zn_{1-x}Cd_xSnS_4$ quinternary alloys nanostructures shows t_{Res} (0.010) and t_{Rec} (0.011) for x = 0.6 (Table 3).

4 Conclusion

The $Cu_2Zn_{1-x}Cd_xSnS_4$ quinternary alloys nanostructures are grown on n-PS (63.93 %) using spin coating technique. It is deduced that Cd contents correlate directly with lattice constant and inversely with bulk modulus, that reflect the stiffness of $Cu_2Zn_{1-x}Cd_xSnS_4$ quinternary alloys nanostructures. The band gap is found to decrease with increasing Cd contents. Photocurrent measurements show the highest photoresponse for $Cu_2Zn_{0.4}Cd_{0.6}SnS_4$ quinternary alloys nanostructures.

Acknowledgments Y. A. would like to acknowlegde University Malaysia Perlis for Grant Nos. 9007-00111 and 9007-00185 and TWAS-Italy for the full support of his visit to JUST-Jordan under TWAS-UNESCO Associateship. K. D. V. would like to acknowledge U. G. C., New Delhi, India for providing financial assistance in the form of Major Research Project [Code: 42-856/2013(SR)]. A. H. R. would like to acknowledge the CENTEM Project, Reg. No. CZ.1.05/2.1.00/03.0088, cofunded by the ERDF as part of the Ministry of Education, Youth and Sports OP RDI programme and, in the follow-up sustainability stage, supported through CENTEM PLUS (LO1402) by financial means from the Ministry of Education, Youth and Sports under the "National Sustainability Programme I". Computational resources were provided by MetaCentrum (LM2010005) and CERIT-SC (CZ.1.05/3.2.00/08.0144) infrastructures.

References

Abd HR, Al-Douri Y, Ahmed NM, Hashim U (2013) Alternative-current electrochemical etching of uniform porous silicon for photodetector applications. Int J Electrochem Sci 8:11461–11473

Al-Douri Y (2003) The pressure effect of the bulk modulus seen by the charge density in CdX compounds. Mater Chem Phys 78:625–629

Al-Douri Y (2012) Confirmation of bulk modulus model of III–V compounds under pressure effect using tight-binding method. Optik Int J Light Electron Opt 123:989–992

Al-Douri Y, Abid H, Aourag H (2002) Calculation of bulk moduli of semiconductor compounds. Physica B 322:179–182

Al-Douri Y, Abid H, Aourag H (2004) Empirical formula relating the bulk modulus to the lattice constant in tetrahedral semiconductors. Mater Chem Phys 87:14–17

Al-Douri Y, Abid H, Aourag H (2005) Correlation between the bulk modulus and the transition pressure in semiconductors. Mater Lett 59:2032–2034

Al-Douri Y, Ahmed NM, Bouarissa N, Bouhemadou A (2011) Investigated optical and elastic properties of Porous silicon: theoretical study. Mater Des 32:4088–4093

Canham LT (1990) Silicon quantum wire array fabrication by electrochemical and chemical dissolution of wafers. Appl Phys Lett 57:1046–1048

Canham LT (1997) Properties of porous silicon. Malvern, Dera, UK

Cláudia RB, Maurício RB, Antonio FB, Neidenêi GF (2008) Morphological and optical characteristics of porous silicon produced by anodization in HF-ethanol solutions. J Braz Chem Soc 19:76–82

Cohen ML (1985) Calculation of bulk moduli of diamond and zincblende solids. Phys Rev B 32:7988–7995

Daranfed W, Aida MS, Attaf N, Bougdir J, Rinnert H (2012) Cu2ZnSnS4 thin films deposition by ultrasonic spray pyrolysis. J Alloy Compd 542:22–27

Guan H, Zhao J, Wangi X, Yu F (2013) Cu_2CdSnS_4 Thin film prepared by a simple solution method. Chalcogenide Lett 10:367–372

Guo QJ, Hillhouse HW, Agrawal R (2009) Synthesis of Cu_2ZnSnS_4 nanocrystal ink and its use for solar cells. J Am Chem Soc 131:11672–11673

Harison WA (1989) Electronic structure and the properties of solids. General Publishing Company, Toronto

Hong S, Kim C (2013) Characteristics of Cu_2ZnSnS_4 Thin Films Fabricated by Sulfurization of Two Stacked Metallic Layers. Mol Cryst Liq Cryst 602:134–143

Hu L, Brewster MM, Xu X, Tang C, Gradečak S, Fang X (2013) Heteroepitaxial growth of GaP/ZnS nanocable with superior optoelectronic response. Nano Lett 13:1941–1947

Ibraheam AS, Al-Douri Y, Hashim U, Ghezzar MR, Addou A, Ahmed WK (2015) Cadmium effect on optical properties of $Cu_2Zn_{1-x}Cd_xSnS_4$ quinternary alloys nanostructures. Sol Energy 114:39–50

Kamoun N, Bouzouita H, Rezig B (2007) Fabrication and characterization of Cu_2ZnSnS_4 thin films deposited by spray pyrolysis technique. Thin Solid Films 515:5949–5952

Katagiri H, Saitoh K, Washio T, Shinohara H, Kurumadani T, Miyajima S (2001) Development of thin film solar cell based on Cu_2ZnSnS_4 thin films. Sol Energy Mater Sol Cells 65:141–148

Katagiri H, Jimbo K, Shwe Maw W, Oishi K, Yamazaki M, Araki H (2009) Development of CZTS based thin film solar cells. Thin Solid Films 517:2455–2460

Lam PK, Cohen ML, Martinez G (1987) Analytic relation between bulk moduli and lattice constants. Phys Rev B 35:9190–9199

Levcenco S, Dumcenco D, Wang YP, Huang YS, Ho CH, Arushanov E, Tezlevan V, Tiong KK (2012) Influence of anionic substitution on the electrolyte electroreflectance study of band edge transitions in single crystal $Cu_2ZnSn(SxSe_{1-x})_4$ solid solutions. Opt Mater 34:1362–1365

Luque PA, Quevedo-Lopez MA, Olivas A (2013) Influence of deposition time on ZnS thin film growth over SiO_2 and glass substrates. Mater Lett 106:49–51

Matsushita H, Maeda T, Katsui A, Takizawa T (2000) Thermal analysis and synthesis from the melts of Cu-based quaternary compounds Cu-III-IV-VI4 and Cu_2-II-IV-VI4 (II¼ Zn, Cd; III¼Ga, In; IV¼Ge, Sn; VI¼Se). J Cryst Growth 208:416–422

Menna P, Francia GD, Ferrara VL (1997) Porous silicon in solar cells: a review and a description of its application as an AR coating. Solar Energy Mater Solar Cells 37:13–19

Phillips JC (1973) Bonds and bands in semiconductors. Academic Press, San Diego

Schirone L, Sotgiu G, Montecchi M, Parisini A (1997) Porous silicon in high efficiency large area solar cells. In: Proceedings of the 14th European PV solar energy conference, p 1479

Schirone L, Sotgiu G, Montecchi M, Righini G, Zanoni R (1998) Stain etched porous silicon technology for large area solar cells. In: Proceedings of the 2nd world conference PV solar energy conversion, p 276

Sherry AM, Kumar M (1991) Analysis of thermal expansion for alkali halide crystals using the isobaric equation of state. J Phys Chem Solids 52:1145–1148

Maeda T, Nakamura S, Wada T (2012) First-principles study on Cd doping in Cu_2ZnSnS_4 and $Cu_2ZnSnSe_4$. Jpn J Appl Phys 51:10NC11. doi:10.1143/JJAP.51.10NC11

Tallon JL (1980) The thermodynamics of elastic deformation—I: equation of state for solids. J Phys Chem Solids 41:837–850

Todorov TK, Reuter KB, Mitzi DB (2010) High-efficiency solar cell with earth-abundant liquid-processed absorber. Adv Mater 22:E156–E159

Xinkun W, Wei L, Shuying C (2012) Photoelectric properties of Cu_2ZnSnS_4 thin films deposited by thermal evaporation. J Semicond 3:22002–22005

Yerokhov VY, Melnyk II (1999) Porous silicon in solar cell structures: a review of achievements and modern directions of further use. Renew Sustain Energy Rev 3:291–299